LAWRENCE
LIVERMORE
NATIONAL
LABORATORY

LLNL-JRNL-659615

CO2 Adsorption on Anatase TiO2 (101) Surfaces in the Presence of Subnanometer Ag/Pt Clusters: Implications for CO2 Photoreduction

C. Yang, B. C. Wood, V. R. Bhethanabotla, B. Joseph

September 2, 2014

Journal of Physical Chemistry C

Disclaimer

CO_2 Adsorption on Anatase T_iO_2 (101) Surfaces in the Presence of Subnanometer Ag/Pt Clusters: Implications for CO_2 Photoreduction

Chi-Ta Yang,[1] Brandon C. Wood,[2] Venkat R. Bhethanabotla,[3] Babu Joseph[4]*

[1,3,4]Department of Chemical and Biomedical Engineering, University of South Florida, Tampa, FL, 33620, USA, [2]Quantum Simulations Group, Lawrence Livermore National Laboratory, Livermore, CA 94550, USA.

[1]chita@mail.usf.edu, [2]brandonwood@llnl.gov, [3]bhethana@usf.edu, [4*]bjoseph@usf.edu,

Corresponding Author: *Email: bjoseph@usf.edu. Phone: 813-974-0692.

Keywords: Ag/Pt Subnanometer Clusters, CO_2 Photoreduction, Density Functional Theory, CO_2 Dissociation to CO, Photocatalysis

Abstract

Using Density Functional Theory calculations, we show how CO_2 adsorption on perfect and reduced anatase TiO_2 (101) surfaces can be substantially modified by the presence of surface Ag and Pt octamer clusters. We find that adsorption is affected even at sites where the adsorbate is not in direct contact with the octamer, which appears to be a manifestation of an electrostatic competition between attractive (Ti-O) and repulsive (Ti-C) interactions as well as charge donation to CO_2 from the Ag/Pt-modified surface. In addition, TiO_2-supported Pt octamers offer key advantages that could be leveraged for CO_2 photoreduction, including providing additional stable adsorption sites for bent CO_2 species and facilitating charge transfer to aid in CO_2^- anion formation. Electronic structure analysis suggests these factors arise primarily from the hybridization of the bonding molecular orbitals of CO_2 with d orbitals of the Pt atoms. Our results show that for adsorption on TiO_2-supported Pt octamers, the O-C-O bending and C-O asymmetric stretching frequencies can be used as reliable indicators of the presence of the CO_2^- anion intermediate, as well as to distinguish unique adsorption geometries/sites. Finally, we suggest a possible pathway for subsequent CO_2 dissociation to CO at the surface of a reduced anatase TiO_2 (101)-supported Pt octamer, which has a computed energy barrier of 1.01eV.

1. Introduction

Ever since Fujishima and Honda first demonstrated the use of TiO_2 electrodes for photocatalytic water splitting in 1972,[1] numerous researchers have extended into applications such as photocatalytic degradation of environmental harmful species,[2] and photoreduction of CO_2 into light hydrocarbons.[3] However, the efficiency of the photo-conversion remains a weakness.[4] One technique to improve the photo-efficiency is to deposit noble metal nanoparticles on the

semiconductor surface.[5-6] The nanoparticles serve as cocatalysts to reduce the recombination of e-/h+ pairs, or as plasmonic particles to increase the concentration of photoexcited electrons.[7-8] However, cost is a concern for this technique; for example, Pt has proven to be an effective cocatalyst but is expensive and limited in supply. Doping the semiconductor with elements such as N[9-10] and Ag[11] and introducing surface defects are other techniques for improving the photo-efficiency by reducing the bandgap, but they also increase the chances for recombination of e-/h+ pairs.[12]

The addition of subnanometer metal clusters consisting of several atoms represents an alternative strategy that can substantially reduce the materials requirements associated with larger cocatalyst particles. Such clusters have shown enhanced catalytic activity for a variety of reactions such as direct propylene epoxidation,[13] CO oxidation,[14-16] and oxidative dehydrogenation of propane.[17] The promotional effects are attributed to the dynamic structural fluxionality,[16] larger fraction of under-coordinated surface atoms,[17] and the interactions between deposited cluster and the support.[18] In addition, such clusters can potentially introduce extra electronic states within the bandgap (sub-bandgap states) of the semiconductor, thereby reducing the optical absorption gap.[19-22]

While TiO_2 may not prove to be the optimal catalyst for CO_2 photoreduction, TiO_2-based materials continue to provide common settings to understand the chemistry of CO_2 photoreduction.[23] One proposed mechanism starts with the absorption of an incident photon to form Ti^{3+}- O^- sites, followed by the interaction of the Ti^{3+} atoms with CO_2 to form CO_2^-, the latter being the first and key step of the reduction mechanism.[4, 24] The adsorbed CO_2^- then reacts with an $H\cdot$ radical to generate CO, HCO_2H, CH2CO, CH_3OH, and CH_4. The success of the key step (reduction of CO_2 to CO_2^-) relies on the geometry with which CO_2 is adsorbed on the TiO_2

surface: the more bent the geometry of the adsorbed CO_2 molecule, the easier the transfer of photoexcited electrons to CO_2 to form the CO_2^- anion.[25-27] This is due to the decrease of the CO_2 LUMO energy as the O-C-O bond angle decreases.[28] Prior quantum mechanical calculations have investigated CO_2 adsorption on the electronic ground or excited states of different surfaces of TiO_2 clusters.[26, 29-30] More thorough studies have considered CO_2 adsorption on periodic TiO_2 anatase (101) surfaces, including the effect of oxygen vacancies or interstitial Ti atoms at surface or subsurface sites.[25, 31]

In this article, we extend previous work by using density functional theory (DFT) to examine the interplay between CO_2 adsorbates and anatase TiO_2 (101) surfaces in the presence of subnanometer Ag & Pt clusters, which we represent by octamers. The choice of surface was motivated by the fact that anatase is the dominant crystal structure of TiO_2 in a commercial Degussa P25 photocatalyst (80% anatase and 20% rutile), and the (101) surface is the most stable anatase surface.[32] In addition, scanning tunneling microscopy (STM) points to the existence of various point defects such as oxygen vacancies, hydroxyl groups, and interstitial atoms, which may bring important effects to the interaction between the surface and the metal clusters;[33] accordingly, we consider the possible presence of a surface oxygen vacancy (i.e., reduced surface) in addition to the pristine anatase surface.

Specifically, we frame our discussion according to four basic ingredients for designing an effective CO_2 photoreduction catalyst (focusing here on the formation of key reaction precursors): (i) availability of binding sites, (ii) intermediate adsorption energy at those sites (too strong = traps; too weak = inactive), (iii) bent geometry of CO_2, and (iv) localized charge transfer to CO_2 to facilitate CO_2^- formation. We investigate the impact that adding Ag and Pt clusters to anatase surfaces has on each of these four factors. The geometry and energetics of CO_2 adsorption are

first examined in detail using electronic structure techniques. The CO_2 adsorption modes are then correlated with calculated vibrational frequencies to provide a roadmap for interpreting and characterizing IR spectra. Finally, a possible dissociation mechanism of CO_2 to CO (in its precursor state) on one of our tested surfaces is discussed. This understanding is intended to guide the design of promising subnanometer metal cluster/semiconductor catalyst frameworks for CO_2 photoreduction.

2. Computational Methods

Titanium atoms on the anatase TiO_2 (101) surface consist of 5-fold(5c-) and 6-fold(6c-) coordinated Ti atoms, whereas the surface oxygen atoms comprise 2-fold(2c-) and 3-fold(3c-) coordinated O atoms. The 3c-O atoms can be further decomposed into 3c-O between 5-fold coordinated Ti and between 6-fold coordinated Ti atoms.[21, 34] The reduced surface is modeled by removing an oxygen atom from a bridge site (2c-O), resulting in conversion to 4c-Ti and fewer exposed 5c-Ti atoms. The stable configurations of perfect and reduced surface-supported Ag and Pt octamers were obtained by following the procedures from our previous work.[21]

The DFT calculations were performed with the Perdew–Burke–Ernzerhof (PBE) functional of the generalized gradient approximation (GGA)[35] using the VASP (Vienna Ab Initio Simulation package) code.[36-38] The electron-ion interactions were modeled by the projector-augmented wave (PAW)[39] method. A kinetic energy cutoff of 500 eV was used for the wavefunctions, and energies were converged to 10^{-5} eV. Spin polarized calculations were incorporated in the geometry optimization, with the force convergence criteria on each atom set to < 0.01 eV/ Å. A 3x1 supercell of the anatase TiO_2 surface with six trilayers was considered. Among the six trilayers, the bottom three layers were frozen, while the top three layers and metal clusters were allowed to relax. A Monkhorst-Pack [40] mesh of 2x2x1 k-points was used to sample

the Brillouin zone for determining the adsorption geometry of CO_2 on the model surfaces; this was increased to 6x6x1 for the density of states (DOS) calculations. The vacuum region between the slabs was set to 12 Å. The adsorption energy of CO_2 was calculated as the difference between the total energy of the CO_2 adsorbed on the model surfaces, and the sum of energies of the isolated CO_2 and model surfaces. Within this definition, an more negative adsorption energy indicates more favorable adsorption.

To study the electronic structure of the interactions of CO_2 with the model surfaces, we computed atom-projected densities of states (p-DOS) within the energy range of interest (from the level of the bonding molecular orbitals of CO_2 to 1 eV above the Fermi level), as well as density plots (DPs) with equal-density isosurfaces of 0.001e/ $Å^3$. The zero energy position in each p-DOS figure within this work corresponds to the Fermi level. Charge population changes upon CO_2 adsorption on the model surfaces were analyzed using Bader charge analysis.[41] The climbing image nudged elastic band method (CI-NEB)[42-44] (Γ point sampling and spin restricted) was used to investigate the mechanism of CO_2 dissociation to CO. The vibrational frequencies were calculated using the frozen-phonon approach with a displacement of 0.015 Å for the C and O atoms of the CO_2 molecule.

3. Results and Discussion

3.1 CO_2 Adsorption on TiO_2 Surfaces

We begin with a discussion of CO_2 adsorption on perfect and reduced anatase TiO_2(101) surfaces without Ag or Pt clusters. On the perfect anatase TiO_2 (101) surface, three CO_2 adsorption modes were identified: one linear (L1) and two bent (B1, B2) forms; on the reduced surface (Vo), six modes were obtained: one linear (LVo1) and five bent (BVo1-BVo5) forms. Among the adsorption modes, B1, B2, and BVo5 were found to be slightly metastable. The optimized

geometries and corresponding structural parameters are given in Fig. S1 of the Supporting Information. Table 1 shows the corresponding adsorption energies, O-C-O angles of CO_2, and changes in the Bader charge of the CO_2 molecule and of its central C atom. Our computed configurations are almost the same as those reported by He et al. (using VASP with the PBE functional)[25] and by Sorescu et al. (using VASP with PBE with corrections for the long-range dispersion interactions).[31] Compared to the results obtained by He et al.,[25] the trends in the adsorption energy and structural parameters for binding on the perfect surface are the same, though our adsorption energies are a bit weaker; this may be due to a different convergence criterion and supercell size. Compared to the study by Sorescu et al.,[31] our converged configurations and the trends in the adsorption energy on both perfect and reduced surfaces are also quite similar, except for BVo4, for which we obtained a somewhat larger O-C-O angle.

Comparing the energies in Table 1 to the geometries in Fig. S1 reveals site-specific trends of the binding mechanism. The O atom in CO_2 tends to bind with surface Ti atoms, whereas the C of CO_2 tends to bind with surface O atoms. Specifically, on the perfect surface, the preference is for the O atom of CO_2 to bind with 5c-Ti, while on the reduced surface it also binds with 6c-Ti. The latter effect is likely due to the greater exposure of 6c-Ti surface sites in the presence of the oxygen vacancy, which results from the vacancy-induced modification of the local surface structure. The O atom's tendency to bind with both 5c-Ti and 6c-Ti on a reduced surface is best illustrated by BVo1, in which it binds to both sites simultaneously; this is also the most stable of all of our tested configurations. The C atom in CO_2 favors binding with either 2c-O and 3c-O (5Ti) on the perfect surface, whereas on the reduced surface 3c-O (6Ti) also becomes possible (e.g., BVo3, for which the C-to-3c-O binding distance is 1.41Å).

On average, the introduction of oxygen vacancies appears to have two key effects on CO_2 adsorption: first, it increases the number of possible CO_2 binding configurations; and second, it enhances the adsorption strength on the surface. This second point is particularly evident when comparing the metastable B2 with the highly stable BVo2, which is analogous except for the removal of a bridging oxygen. The oxygen vacancy helps stabilize CO_2 adsorption in BVo2, likely because CO_2 gains electron density from the oxygen vacancy (0.088e). We emphasize that such negative charge accumulation at the C of CO_2 is crucial to the formation of the CO_2^- anion for CO_2 photoreduction,[25] and is particularly pronounced for BVo1 and BVo4 (0.827e and 0.421e, respectively).

Table 1. Calculated properties[a] based on stable adsorption configurations of CO_2 on perfect/reduced anatase TiO_2(101).

Ads. config.	$-E_{ads}$(eV)	∠OCO(deg.)	Δe of CO_2	Δe of C in CO_2
B1	-0.02	130.1	-0.011	0.017
B2	-0.09	134.1	0.062	-0.005
L1	0.14	178.7	-0.013	-0.025
BVo1	0.76	135.2	0.799	0.827
BVo2	0.51	132.4	0.088	0.024
BVo3	0.37	127.6	0.150	0.064
BVo4	0.13	150.1	0.393	0.421
BVo5	-0.03	129.9	0.001	-0.005
LVo1	0.36	177.8	-0.036	-0.048

[a] Values represent the adsorption energy, O-C-O angle of CO_2, and the difference of the Bader charge of the CO_2 molecule upon adsorption (Δe >0 means electron accumulation; L and B represent linear and bent adsorption forms; Vo represents an oxygen vacancy).

3.2 CO_2 Adsorption on TiO_2 Supported Ag/Pt Octamers Surfaces

Next, we discuss how the adsorption properties of CO_2 are affected by the presence of the Ag and Pt octamers on anatase TiO_2 (101), focusing on structural and electronic properties, the CO_2 binding mechanism, and the associated vibrational properties. Particular attention is paid to two factors that are directly relevant for catalytic activity: first, the availability of viable surface binding sites for CO_2; and second, the bent geometry and charge accumulation on the adsorbate, which together facilitate CO_2 activation. Note that some reconstruction of the octamer occurs during CO_2 adsorption on both perfect and reduced surfaces; this is due to the fluxionality characteristic of the subnanometer metal cluster, which was discussed in our previous work on the adsorption of Ag and Pt dimers, tetramers, and octamers on the anatase TiO_2 (101) surface.[21]

3.2.1 Structural and Electronic Properties

- Pt/Ag on Perfect Anatase (101) Surface

We begin by considering CO_2 binding on perfect (vacancy-free) anatase (101) surfaces with Ag and Pt octamers. The optimized configurations and structural parameters of CO_2 adsorption for this case are given in Figure 1. The adsorption energy, O-C-O angle of CO_2, and Bader charge difference of the CO_2 molecule upon adsorption for each of the configurations of Figure 1 are reported in Table 2. In the presence of the Ag octamer, two bent (BA1 and BA2) and one linear (LA1) CO_2 adsorption modes were found, as shown in Figure 1a-c. In the presence of the Pt octamer, four bent (BP1-BP4) and one linear (LP1) CO_2 adsorption modes were found, as shown in Figure 1d-h. The adsorption configurations can be broadly classified into two categories: those where CO_2 binds directly to the TiO_2 surface itself (BA2, LA1, BP4, LP1); and those where CO_2 interacts appreciably with the metal cluster (BA1, BP1, BP2, BP3).

Adsorption at TiO_2 sites (with octamer present). A comparison of Tables 1 and 2 makes it clear that the presence of Ag and Pt octamers affects CO_2 binding even when there is no direct contact between the adsorbate and the metal clusters, i.e., when binding is directly on TiO_2 surface sites (BA2, LA1, BP4, LP1). Moreover, the effect of the Ag & Pt octamers on CO_2 adsorption at these sites varies depending on the orientations of the CO_2 molecule.

To see this, consider the linear modes, LA1 & LP1 (Figure 1c & 1h) and the bridge carbonate-like modes, BA2 & BP4 (Figure 1b & 1g), which are similar to one another in terms of O-C-O angles of CO_2 and binding distances. In comparison with analogous modes on the perfect surface without Ag/Pt (L1 and B2 in Fig. S1a & S1c in Supporting Information), the linear LA1 and LP1 have longer bond lengths between the O atom of CO_2 and the surface Ti atom by up to 0.2 Å (Fig. S1 in Supporting Information and Figure 1), as well as weaker adsorption energies (refer to Table 1 & 2). Conversely, the presence of Ag or Pt octamers stabilizes the metastable bent B2 configuration, strengthening adsorption for the stable BA2 and BP4 bent configurations (which have nearly identical structural parameters).

The Bader charge analysis in Table 2 indicates that the additional negative charge accumulated on the binding O atom of CO_2 for LA1 (0.026e) and LP1 (0.061e) sustains binding with the surface Ti atom, similar to the value found for L1 on the undecorated surface (0.033e). BA2 and BP4 also show net significant electron accumulation in both O atoms of CO_2 upon binding. However, though qualitatively consistent with B2 on the undecorated surface (Table 1), the magnitude of this accumulation is much greater for BA2 and BP4. Moreover, the electron accumulation on the O atoms of CO_2 for BA2 and BP4 is not accompanied by any significant electron depletion on the C atom, indicating charge is being transferred from the substrate rather than internally redistributed within the CO2 molecule. This behavior may explain the

transformation from the metastable B2 to stable BA2 and BP4 upon addition of Ag/Pt. The localized net charge at both O atoms of CO_2 facilitates binding with the surface Ti atom, which agrees with the result reported by He and coworkers.[25] The enhanced electron density in the CO_2 adsorbate derives from the tendency of Ag & Pt octamers to donate electrons to the anatase (101) surface: our previous work suggests that Ag and Pt octamers have the tendency to donate electron to the anatase (101) surface (1.075 and 0.450e).[21] Similar trends have also been observed on model surfaces of Pt dimers on rutile TiO_2 (110)[45], Ag(2,4,8) on anatase (110)[46], and Pt(1-3) on anatase (101)[19]. The enhanced CO_2 adsorption phenomenon is similar to the observation that O_2 adsorption on stoichiometric rutile TiO_2 (110) becomes favored when electronic density is transferred from deposited small Au clusters to the oxide.[47]

Adsorption at sites associated with octamers. Examination of the sites for which CO_2 binds in direct contact with the Ag/Pt octamers (BA1, BP1, BP2, BP3) reveals two additional facts. First, we find that the presence of the Pt octamer exposes more additional CO_2 adsorption sites than does the presence of the Ag octamer (three for Pt vs. one for Ag). Second, CO_2 tends to adsorb rather strongly on the Pt site.

BA1 (Figure 1a) is the sole Ag octamer-associated CO_2 adsorption site, in which CO_2 binds at the interface between the Ag octamer and the TiO_2 surface with a distance of 2.26 Å between O(a) and the nearest Ag atom. Compared to analogous modes without the octamer (B1 in Fig. S1b in Supporting Information), there is an increase of the C-O bond length in CO_2 by 0.04 Å; the O-C-O angle of CO_2 is also smaller. The elongation is attributed to the interaction of the Ag octamer with CO_2, indicated by increased charge transfer to O(a) for BA1 (0.072e) compared to B1 (0.042e). The additional charge transfer also explains the increase in adsorption strength by 0.33eV, and reveals the Ag octamer's role in stabilizing CO_2 on the surface in this mode.

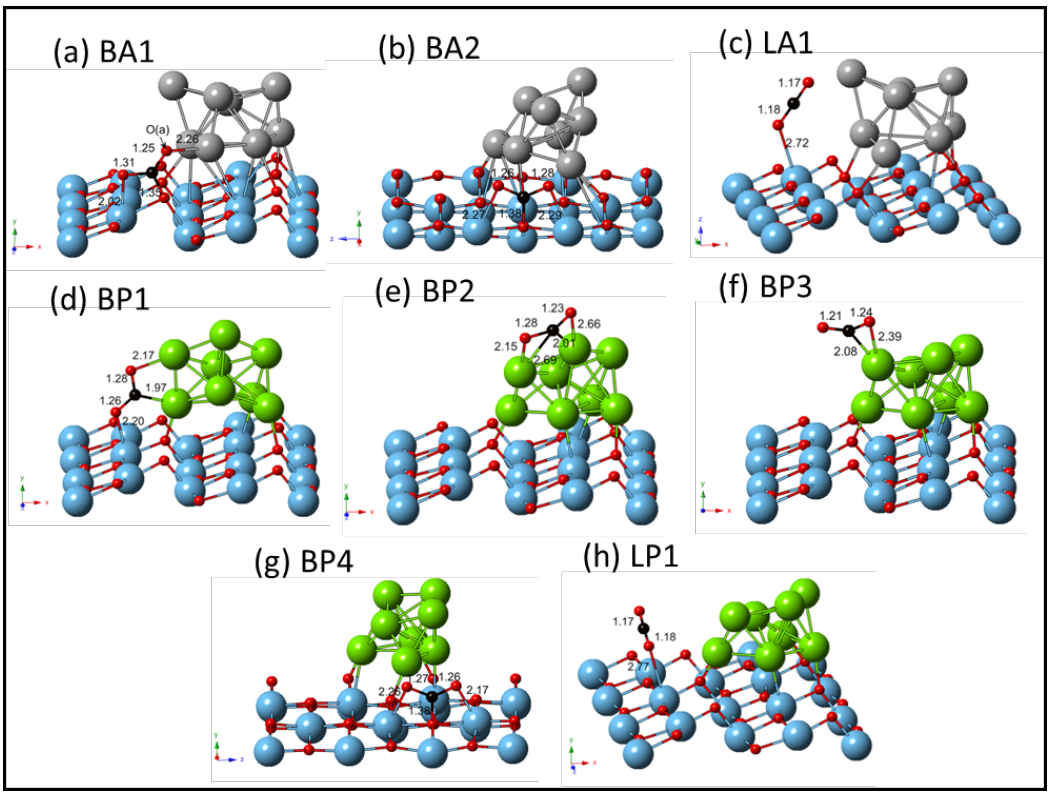

Figure 1. Stable CO_2 adsorption configurations on the perfect anatase TiO_2(101) surface in the presence of Ag and Pt octamers (O in red, C in black, Ti in blue, Ag in silver, Pt in green. The numbers indicate the bond lengths in Å).

The three additional CO_2 adsorption sites provided by the Pt octamer for bent-form CO_2 are BP1-BP3 (Figure 1d-f). BP1 represents CO_2 adsorption at the interface edge of the Pt octamer and TiO_2 surface. In this configuration, CO_2 binds with 5c-Ti using one of its O atoms, while using C and the other O to bind with the Pt octamer. On the other hand, in BP2 and BP3, CO_2 adsorbs solely on the Pt octamer, with no direct interaction with the anatase surface; notably, these configurations are unique to Pt, with no analog for Ag. In BP2, the C atom of CO_2 bridges two Pt atoms, each of which also interacts with a different O atom of CO_2. In BP3, the CO_2 molecule uses C and one O to bind with one Pt atom.

On average, adsorption on the three Pt sites is stronger than on the surface with supported Ag octamers or on the clean perfect anatase surface, which means that the supported Pt octamer surface will tend to enrich the adsorbed CO_2 species. Moreover, BP1, BP2, and BP3 show a tendency for significant negative charge accumulation in the C atom of CO_2 (0.599, 0.537, and 0.374e, respectively), which is favorable for formation of the CO_2^- anion. The charge accumulation can also be easily observed in the charge density difference of BP1 and BP2 (see Fig. S2 in Supporting Information). Note that the O-C-O angle of CO_2 decreases as the net charge transfer and the adsorption strength increase. In fact, the O-C-O angles of adsorbed CO_2 in BP1 and BP2 are close to the reported angles of the CO_2^- anion based on experimental and theoretical results, 127±8° and 138°, respectively.[25] We point out that the C atom's acquisition of additional negative charge is similar to the electronic behavior of adsorption modes found on clean perfect Zn_2GeO_4 (010) and (001) surfaces.[48] This reveals that depositing subnanometer metal clusters can bring new electronic properties to a conventional photocatalyst such as TiO_2, and that a Pt octamer deposited on perfect anatase (101) has the capability to activate the CO_2 molecule. Notably, this behavior contrasts with CO_2 adsorption modes on clean perfect anatase TiO_2 (101)[25], perfect brookite (210)[49], and perfect ceria (110)[50] where no stable bent form of CO_2 or net charge accumulation on C upon adsorption were found.

Table 2. Calculated properties[a] based on CO_2 adsorption configurations on perfect anatase TiO_2(101) in the presence of Ag and Pt octamers.

Ads. config.	$-E_{ads}$(eV)	∠OCO(deg.)	Δe of CO_2			ν(CO_2)(cm^{-1})		
			C	O	O	ν1	ν2	ν3
BA1*	0.31	126.1	-0.012	-0.018	0.072	1213	827	1606
BA2	0.20	132.7	0.001	0.077	0.102	1247	801	1629
LA1	0.11	178.6	-0.014	0.000	0.026	1317	624	2359
BP1*	0.72	127.7	0.599	0.044	-0.051	1174	760	1511
BP2*	0.69	135.9	0.537	-0.041	-0.053	1130	713	1690
BP3*	0.16	148.4	0.374	-0.058	0.000	1167	602	1918
BP4	0.09	132.2	-0.006	0.054	0.072	1260	806	1615
LP1	0.10	179.0	-0.029	-0.003	0.061	1307	608	2345

[a]Values represent the adsorption energy, O-C-O angle of CO_2, difference of the Bader charge of the CO_2 molecule upon adsorption, and vibrational frequencies of symmetric (ν1), bending (ν2), and asymmetric (ν3) stretching modes (Δe >0 means electron accumulation; L and B represent linear and bent adsorption forms; A and P represent Ag and Pt; asterisks indicate interaction associated with Ag/Pt octamers).

- Pt/Ag on Reduced Anatase (101) Surface

Next, we consider CO_2 binding on reduced anatase (101) surfaces (i.e., oxygen vacancy) with Ag and Pt octamers. Identified CO_2 adsorption configurations and corresponding structural parameters for this case are given in Figure 2. The adsorption energy, O-C-O angle of CO_2, and Bader charge difference of the CO_2 molecule upon adsorption for each of the configurations of Figure 2 are reported in Table 3. On the reduced surface with the Ag octamer, two bent (BAVo1 and BAVo2) and one linear (LAVo1) CO_2 adsorption configurations were found, as shown in Figure 2a-c. In the presence of the Pt octamer, six bent (BPVo1-BPVo6) and one linear (LPVo1) CO_2 adsorption configurations were found, as shown in Figure 2d-j. As we did for the vacancy-free surface, we categorize the configurations into two categories: one where CO_2 binds directly

to the TiO_2 surface (LAVo1, LPVo1, BAVo1, BPVo5), and another where there is direct interaction with the metal cluster (BAVo2, BPVo1, BPVo2, BPVo3, BPVo4, BPVo6).

Adsorption at TiO_2 sites (with octamer present). As we found for the perfect surface, the presence of the Ag or Pt octamer has an impact on TiO_2 sites, even those that are not directly associated with the octamer. However, unlike the perfect surface case, there does not appear to be a significant dependence on the specific orientation of the adsorbed CO_2 molecule.

Again, some insight can be gained by comparing adsorption configurations on the reduced surfaces with Ag/Pt to analogous configurations on the reduced surfaces without the octamer. The linear LAVo1 and LPVo1 configurations (Figure 2c & 2j) are similar structurally, and are closest to LVo1 for the octamer-free surface (Fig. S1d in Supporting Information); nevertheless, these two sites show longer bonding lengths between O of CO_2 and Ti atom by 0.38 Å and 0.29 Å, and less than half the adsorption energy magnitude of the octamer-free surface. For these linear geometries, the net effect of the octamers on CO_2 adsorption is therefore consistent between the reduced and perfect (vacancy-free) surfaces. The bent BAVo1 and BPVo5 (Figure 2a & 2h) geometries, which are almost the same in terms of adsorption configuration, are also less stable compared to the analogous mode on the reduced surface (BVo2 in Fig. S1f in Supporting Information). In other words, the presence of Ag and Pt octamers weakens the CO_2 binding with the reduced surface in this configuration (in fact, BPVo5 becomes a metastable mode). Accordingly, the trend for the bent geometries matches that for the linear geometries, but is the opposite of the trend found in perfect surface-supported octamers. At first glance, this is curious given that the Bader charge analysis also shows negative charge localization at the binding O of the CO_2 molecule upon adsorption in the LAVo1 (0.019e) and LPVo1 (0.033e) configurations. However, this accumulation is much less than what we observed for LVo1 on the

octamer-free surface (0.060e), which is consistent with the relative decrease in adsorption energy, and with the increase in the binding distance of the O atoms of CO_2 and the surface Ti atoms. We caution, however, that BAVo1 and BPVo5 show enhanced net charge transfer in the two binding O atoms compared to BVo2, but do not demonstrate a consistent trend in the adsorption energy; accordingly, significant charge transfer should be seen only as a rough guideline for predicting adsorption.

Adsorption at sites associated with octamers. Like the perfect surface with Pt/Ag, we find that more additional CO_2 adsorption sites are introduced at the Pt octamer than at the Ag octamer (five for Pt vs. one for Ag); note that this difference between the two metals is even more pronounced than we saw with the perfect surface. We also find that although the reduced surface provides more binding sites at the octamer, the presence of the oxygen vacancy does not in general enhance the binding strength of CO2 with respect the Ag/Pt-decorated perfect surface.

The lone Ag binding site, BAVo2 (Figure 2b), is a metastable adsorption site with the C atom of CO_2 binding with 3c-O, and with one O atom of CO_2 interacting with the Ag octamer at a distance of 2.36 Å while the other O atom fills the oxygen vacancy site. This configuration is similar to the corresponding mode on the reduced surface without Ag (BVo3 in Fig. S1g in Supporting Information), but it has a much smaller adsorption energy magnitude (by 0.65eV). This indicates that the Ag octamer's presence mitigates the CO_2 adsorption in this configuration. The net charge on the adsorbed CO_2 is also quite different when the Ag octamer is present: the charge transfer to the O atom of CO_2 in BAVo2 is almost double that in BVo3 (no octamer), while the charge transfer to the C atom is one fifth as large.

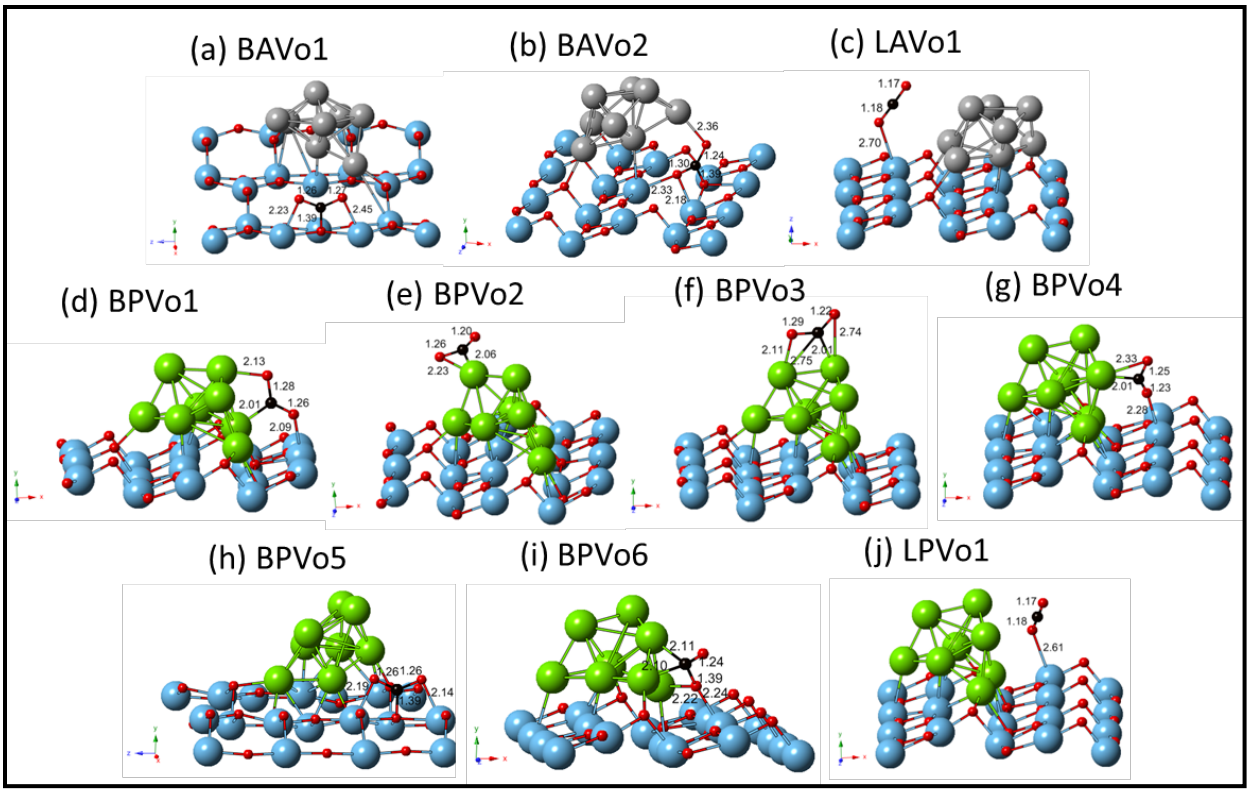

Figure 2. Stable CO_2 adsorption configurations on the reduced anatase TiO_2(101) surface in the presence of Ag and Pt octamers (O in red, C in black, Ti in blue, Ag in silver, Pt in green. The numbers indicate the bond lengths in Å).

Five additional adsorption modes were observed on the reduced surface-supported Pt octamer, two more than were found for the perfect surface-supported case. Configuration BPVo1 (Figure 2d) can be compared to the perfect surface-supported BP1 (Figure 1d), since both sites involve CO_2 adsorption at the interface edge with comparable binding distances of CO_2 to the Pt octamer (albeit with a slight distance decrease by 0.11 Å of the O atom binding to the surface Ti and a smaller O-C-O angle by almost 2.8°). Configuration BPVo2 (Figure 2e) is similar to BP3 (Figure 1f), and mainly involves an interaction with one Pt atom in the top layer; again, both of these configurations possess comparable CO_2 binding parameters except for a 0.16 Å shorter distance between O of CO_2 and the Pt atom. BPVo3 (Figure 2f) is an analogous configuration to BP2 (Figure 1e), and both possess comparable CO_2 binding parameters except for a 1.7° smaller

O-C-O angle for the former. However, BPVo4 (Figure 2g) and BPVo6 (Figure 2i) are unique configurations that have no analog in the perfect surface-supported Pt octamer case. BPVo4 (Figure 2g) shows CO_2 interacting at the interface edge, mainly with one Pt atom in the bottom layer of the octamer. This Pt atom binds the C and O of CO_2, while the other O atom of the adsorbate binds with a 5c-Ti atom, leading to an O-C-O angle of 140.6°. BPVo6 (Figure 2i) is also an interfacial CO_2 adsorption configuration, but a metastable one. In this case, the C atom is interacting with two Pt atoms, while one O atom is simultaneously interacting with one Pt and one surface 5c-Ti atom. Note that among all the CO_2 adsorption configurations obtained in this research, the O-C-O angle in BPVo6 (121.1°) is the smallest, and the binding distance of C and O in CO_2 (1.39 Å) is the longest. Furthermore, this O-C-O angle is smaller than those of the CO_2 anion reported experimentally and computationally, and the C & O intra-bonding distance is larger by around 0.14 to 0.16 Å.[25, 51] This may account for the instability of this mode in terms of total energy, but it also reveals a strong tendency for CO_2 dissociation to occur on this model surface if binding can be achieved.

The adsorption energy for the Pt-derived configurations on the reduced TiO_2-supported Pt octamers is on average comparable to those on the perfect TiO_2-supported Pt octamers. This indicates that the presence of the oxygen vacancy does not contribute to the CO_2 adsorption energetically in the presence of the Pt octamer. However, because additional adsorption sites are introduced by the vacancy-induced modification of the local surface structure, it is likely that the net effect should be to enhance CO_2 photoreduction activity. This assumption is supported by the fact that all five Pt-derived binding configurations (BPVo1-BPVo4 and BPVo6) show a tendency for notable negative charge accumulation in the C atom of CO_2 molecule. Examination of the associated charge density difference plots provides additional confirmation of this effect (plots

for BPVo1 and BPVo2 can be found in Fig. S2 in the Supporting Information). The magnitude of the charge accumulation is comparable to that seen in the modes on the perfect surface-supported Pt octamer, and as in the latter case, appears to correlate with the decreasing O-C-O angle of CO_2 (with one exception for BPVo6). In summary, the reduced anatase TiO_2 (101)-supported Pt octamer surface shows the potential to activate CO_2 by generating the bent form of the molecule, while simultaneously increasing the number of available adsorption sites. This enhanced catalytic capability mirrors our conclusions for clean reduced anatase TiO_2 (101) (BVo1-BVo4), and generally matches observations for Zn_2GeO_4 (010) & (001)[48], brookite (210)[49], and ceria (110)[50] surfaces.

Table 3. Calculated properties[a] based on CO_2 adsorption configurations on reduced anatase TiO_2(101) in the presence of Ag and Pt octamers.

Ads. Config.	$-E_{ads}$(eV)	∠OCO(deg.)	Δe of CO_2			ν(CO_2)(cm^{-1})		
			C	O	O	ν1	ν2	ν3
BAVo1	0.12	132.9	0.009	0.068	0.092	1251	798	1640
BAVo2*	-0.28	128.0	0.012	0.100	0.084	1185	806	1626
LAVo1	0.14	178.8	-0.014	0.002	0.019	1315	626	2359
BPVo1*	0.71	124.9	0.595	-0.058	0.039	1203	772	1529
BPVo2*	0.68	147.6	0.381	-0.086	-0.003	1142	621	1934
BPVo3*	0.66	134.2	0.523	-0.023	-0.065	1114	734	1715
BPVo4*	0.32	140.6	0.417	0.075	-0.077	1180	666	1791
BPVo5	0.00	132.5	-0.007	0.042	0.069	1265	805	1647
BPVo6*	-0.19	121.1	0.566	-0.020	0.009	1145	728	1670
LPVo1	0.15	179.3	-0.020	0.033	-0.009	1318	626	2361

[a]Values represent the adsorption energy, O-C-O angle of CO_2, difference of Bader charge of CO_2 molecule upon adsorption, and vibrational frequencies of symmetric (ν1), bending (ν2), and asymmetric (ν3) stretching modes (Δe >0 means electron accumulation; L and B represent linear and bent adsorption forms; Vo represents an oxygen vacancy; A and P represent Ag and Pt; asterisks indicate interaction associated with Ag/Pt octamers).

3.2.2 Binding Mechanism

Additional insight into the influence of the octamer on CO_2 adsorption can be obtained by investigating the binding mechanism and electronic structure in more detail. We focus on two scenarios that are of particular interest: first, adsorption on perfect and reduced anatase sites for which there is no direct bonding to the octamer; and second, adsorption on the Pt octamer, which introduces the most additional adsorption sties.

Adsorption on TiO_2 sites (with octamer present). Focusing first on sites where CO_2 is not directly bound to the octamer, we find that electrostatics seem to play the dominant role in the binding mechanism. More specifically, there is a competition between attraction and repulsion of CO_2 by surface Ti atoms: CO_2 adsorption on the TiO_2 (101) surfaces is affected by Ti atoms either attracting the O atom of CO_2 or else repelling the C atom.

The Ti-O attraction can be seen by observing the linear adsorption modes for all tested surfaces (refer to L1 & LVo1 in Fig. S1, LA1 & LP1 in Figure 1, and LAVo1 & LPVo1 in Figure 2), for which there is an apparent correlation between the binding strength and the net charge transfer to binding O of the CO_2 molecule. For example, LVo1 has the highest adsorption energy as well as almost the highest net charge on the O atom of CO_2 (0.060e). One exception to this trend is LP1, which has a net charge transfer to O that is comparable to LVo1 (0.061e), yet exhibits much weaker CO_2 binding. This is likely due to the different orientation of the adsorbed CO_2 molecule, as reflected in the variation in the electronic properties of linear modes obtained by Sorescu and coworkers.[31] By comparing LVo1 and LP1, both adsorb along [010] and are surrounded by three surface Ti atoms (more than those of other linear modes), but CO_2 on LP1 lies flatter. This leads to a clear difference in the average distance between the C atom of CO2 and the nearby surface Ti atoms, which is smaller for LP1 (3.89Å) than for LVo1 (4.01 Å). A

likely consequence of this is increased electrostatic repulsion[25] between C and surface Ti atoms in the case of LP1, which results in a smaller adsorption energy.

Such repulsion role of C of CO_2 is also a factor in the binding strength of the bridge carbonate-like configurations (refer to B2 & BVo2 in Fig. S1, BA2 & BP4 in Figure 1, and BAVo1 & BPVo5 in Figure 2), where it competes with the formation of bonding between O atoms of CO_2 and surface Ti atoms. The Bader charge analysis of the pair of BP4 & BPVo5 suggests these two are dominated by the Ti-O bonding effect. Given that C of CO_2 in both modes exhibits the same electronic trend, the difference in the total negative charge accumulation at both O atoms of CO_2 uniquely explains the differences in their binding strength. On the other hand, the pair of B2 & BVo2 illustrates that the charge on the C atom of CO_2 is highly relevant to the binding strength. Whereas the total negative charge accumulations at O of CO_2 are comparable in the two cases (0.067 & 0.064e), the C of CO_2 in BVo2 gains a charge of 0.024e while that in B2 shows an opposite loss of 0.005e. As a result, BVo2 experiences less electrostatic repulsion than B2, which may explain why BVo2 is stable and B2 is metastable. Note that the least favored bridged-carbonate configuration identified in this study is B2, which has both weak binding via O of CO_2 (0.044e less charge accumulation compared to the barely favored BPVo5), as well as electrostatic repulsion between C of CO_2 and surface Ti atoms.

Adsorption at sites associated with Pt octamer. BP1-BP3 (Figure 1d-f) and BPVo1-BPVo6 (Figure 2d-i) reveal the Pt octamer's ability to provide additional adsorption sites for bent-form CO_2 species on anatase TiO_2 (101). This can be explained in terms of the electronic structure of the Pt surface with respect to the adsorbate states, which facilitates the formation of bonding states. Figure 3 shows p-DOS plots for BP1 and BP2, superimposed with select charge density plots corresponding to specific states. The peaks corresponding to Pt and O of CO_2 show

strong resonance at lower energy levels, as well as weaker resonances near the top of the valance band and in the bandgap. For Pt and C of CO_2 atoms, the resonant peaks lie mainly in the lower energy levels, with minor resonances elsewhere, especially in the range of -2eV to Fermi level. This suggests the adsorbed CO_2 has a strong tendency to hybridize with the Pt octamer at lower energy levels (around -10 eV ~ -6eV with respect to the Fermi level). Further examination of the charge density associated with DP1-DP4 (Figure 3a) and DP1&DP2 (Figure 3b) shows that CO_2 is using its bonding molecular orbitals (e.g. $2\sigma_g$ for DP1 in Figure 3a and $1\pi_u$ for DP2 in Figure 3b) to form additional bonding orbitals with d-like orbitals of the Pt octamer. At higher energies, additional orbital hybridization between C and the Pt octamer is observed, as can be seen in the charge densities associated with the DP3&DP4 states in Figure 3b. The ability of CO_2 to form a bonding orbital with the Pt octamer is attributable to the matching shapes, orientations, and comparable energy levels of the two sets of orbitals.[21] It can be concluded that the additional CO_2 adsorption sites provided by Pt octamer are made possible by the ability of Pt to form bonding orbitals with CO_2 molecule. In other words, the dominant binding mechanism for CO_2 on the Pt sites involves orbital hybridization (covalency), whereas electrostatic interactions dominate at sites associated with the TiO_2 surface.

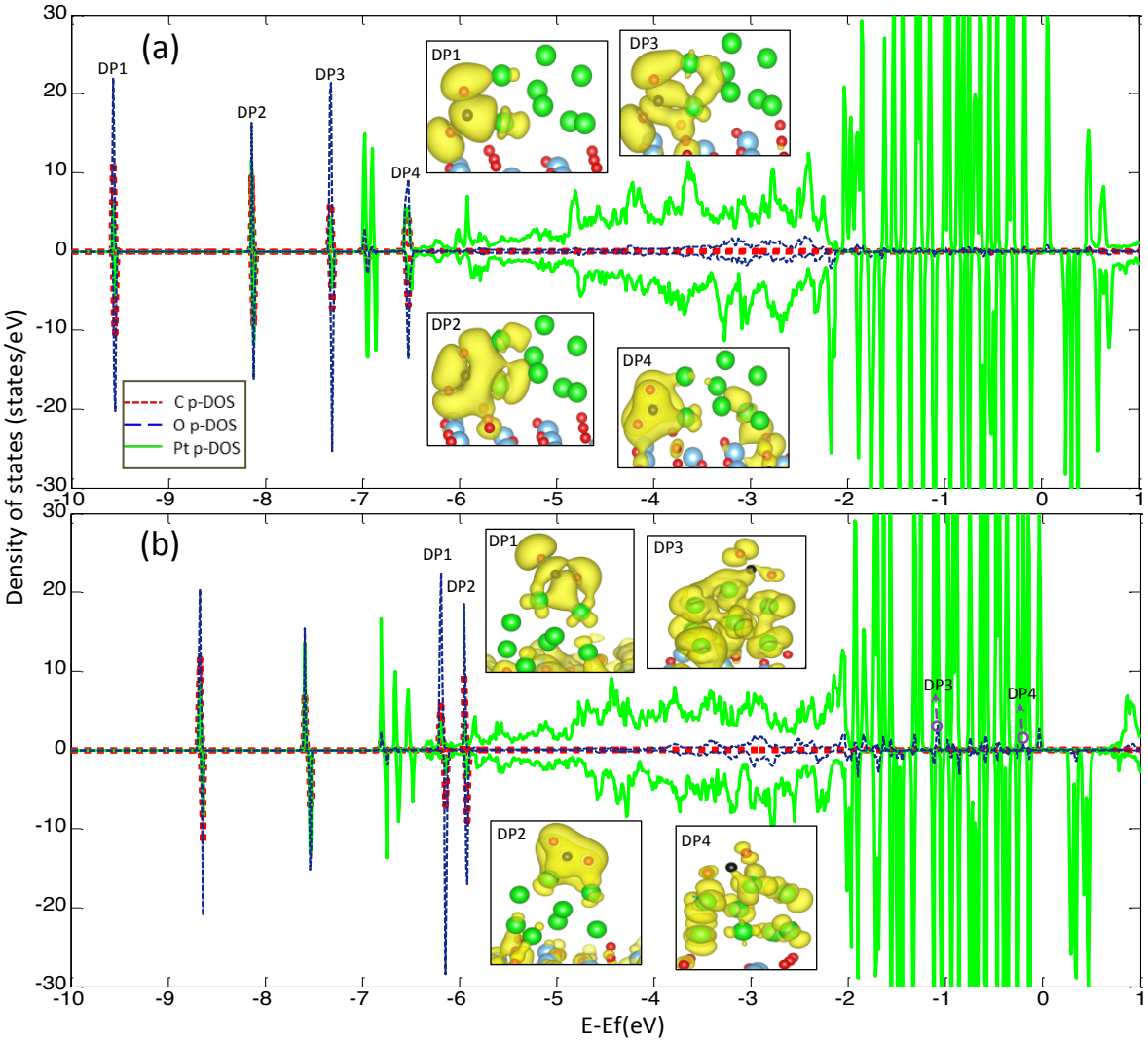

Figure 3. p-DOSs (C & O of CO_2 and Pt) and associated density plots of specific states formed upon CO_2 adsorption at the interface edge (BP1) and directly on the Pt octamer (BP2): (a) configuration BP1 with states DP1-DP4 at -9.57, -8.13, -7.32, and -6.53 eV; (b) configuration BP2 with states DP1-DP4 at -6.17, -5.93, -1.10, and -0.13 eV (Above and below the axis correspond to spin up and spin down, respectively).

3.2.3 Vibrational Frequencies

Analyzing the CO_2 vibrational frequencies on the surfaces with Ag/Pt octamers offers insight into key bond characteristics of the adsorbed molecule, and can provide a useful roadmap for interpreting experimental vibrational spectra. Table 2 & 3 shows the calculated vibrational frequencies for CO_2 adsorbed on surfaces of anatase (101)-supported Ag and Pt octamers.

Significantly, we find that specific vibrational modes can be used as indicators for key geometric and electronic quantities that are directly relevant for CO_2 activation. In particular, among the Pt octamer-associated bent-form CO_2 molecules, there is a correlation between the bending frequency (ν2) and negative charge accumulation at C, and between the asymmetric stretching frequency (ν3) and the O-C-O angle of the adsorbed CO_2 molecule. Moreover, characteristics of the ν2 and ν3 modes may reveal different CO_2 adsorption sites.

The experimental vibrational frequencies of symmetric (ν1) and asymmetric (ν3) stretching for linear adsorbed CO_2 on P25 and several metal oxide surface were reported to be around 1259 and 2373 cm^{-1},[52-53] while frequencies for adsorbed bent-form CO_2 were reported to be 1315 and 1589 cm^{-1} on anatase TiO_2.[54] For the CO_2^- anion, the reported values are 1219 and 1640 cm^{-1} on P25,[53] 1245 and 1670 cm^{-1} on anatase TiO_2,[54] and 1247 and 1670 cm^{-1} on anatase TiO_2 in the presence of H_2O.[55] Previous calculation results[25, 31, 49] revealed that on neutral perfect anatase TiO_2 (101) and brookite TiO_2 (210) surfaces, the calculated vibrational frequencies of the bent CO_2 modes were close to the experimental results, although the electronic analysis prevented the actual formation of CO_2^- anion. For the reduced surfaces, the formation of CO_2^- anion was found, with the calculated vibrational frequencies showing a comparable or slightly larger shift with respect to the experimental values. The relatively good agreement between theory and experiment justifies comparison of our results to published data.

As described above, significant electron transfer to the CO_2 adsorbate was mainly found on the perfect and reduced TiO_2 surfaces in the presence of the Pt octamer. The most promising configurations for CO_2 activation are BP1 - BP3 in Figure 1d-f and BPVo1 - BPVo4 in Figure 2d-g, since these exhibit sufficient electron transfer so as to be close to an adsorbed CO_2^- anion. Calculated vibrational frequencies indicate that the corresponding IR bands for the adsorbed CO_2

are obtained in the range of 602-1934 cm^{-1}. Compared to the reported experimental values for CO_2 on anatase TiO_2, ν1 modes show redshifts up to 131 cm^{-1}, while for ν3 the largest redshift is around 159 cm^{-1} and the largest blueshift around 264 cm^{-1}. The ν2 (bending) mode varies from 602 to 805 cm^{-1}. Note that ν1 and ν3 (1130 and 1690 cm^{-1}) of BP2 are the closest to the experimentally reported values for anatase.

Among the Pt octamer-associated CO_2 adsorption modes (BP1 - BP3 in Figure 1d-f and BPVo1 - BPVo4 in Figure 2d-g) in which the C atom gains appreciable negative charge, a clear trend between the ν2 mode and the charge accumulation at C was found, as shown in Figure 4a. Higher electron accumulation at C is correlated with a higher ν2 mode. This may be related to increased stiffness of the intra C-O bond of CO_2 due to the dipole moment enhancement from the charge transfer to C. Notably, the ν2 mode was also used by He et al.[25] to characterize the net charge transfer to C associated with CO_2 adsorption on the clean anatase TiO_2 (101) surface. Also, Figure 4a shows that in general, interface edge adsorption sites (in red circle, excepting BPVo4) tend to possess higher ν2 modes compared to adsorption sites directly on the Pt octamer (in green dotted circle). Furthermore, if we compare the Pt octamer-associated CO_2 adsorption modes in Figure 4a with modes not directly associated with the Pt octamer (BP4 in Figure 1g and BPVo5 in Figure 2h), the former tend to have ν2 modes below ~800 cm^{-1} while the latter tend to have ν2 modes above that value. This is likely because C interacts with different atoms in these two cases. In the direct interaction of C with Pt atoms, there is noticeable net charge transfer to C and hybridization with the Pt states, which induces a stronger interaction and an associated reduction in the frequency of the bending mode. In contrast, TiO_2 surface sites exhibit a much weaker interaction between C and surface O atoms, involving comparatively minor charge transfer; this accounts for the higher frequency of the CO_2 bending.

The ν3 asymmetric stretching mode for the surfaces with Pt octamers correlates well with the O-C-O angle of the adsorbed CO_2 molecule. As shown in Figure 4b, the smaller the angle, the smaller the value of ν3 (note that this trend holds true even for configurations where charge transfer to C is minimal, i.e., BP4 and BPVo5). For the bent forms on the perfect surface in the presence of the Pt octamer (BP1-BP4 in Figure 1d-g), ν3 decreases as 1918, 1690, 1615, and 1511 cm^{-1}, and the O-C-O angle as 148.4, 135.9, 132.2, and 127.7°. Similarly, on the supported reduced surface (BPVo1 - BPVo5 in Figure d-h), ν3 decreases as 1934, 1791, 1715, 1647, and 1529 cm^{-1}, and the O-C-O angle decreases as 147.6, 140.6, 134.2, 132.5, and 124.9°. Apparently, the smaller O-C-O angle mitigates the antisymmetric stretching of the CO_2 molecule. Moreover, comparing the adsorption modes on the Pt octamer with those at the interface edge, the latter tend to possess a smaller O-C-O angle, and a correspondingly lower ν3 frequency. This is due to the cliff-like geometry created at the interface between the Pt octamer and the anatase (101) surface, which allows CO_2 to adsorb with an O-C-O angle that approaches 90°. Excepting BPVo4, we suggest that a smaller value of ν3 (~1500-1540 cm^{-1}, red circle in Figure 4b) could be used as a signal that CO_2 is adsorbed at the cluster/support interface edge.

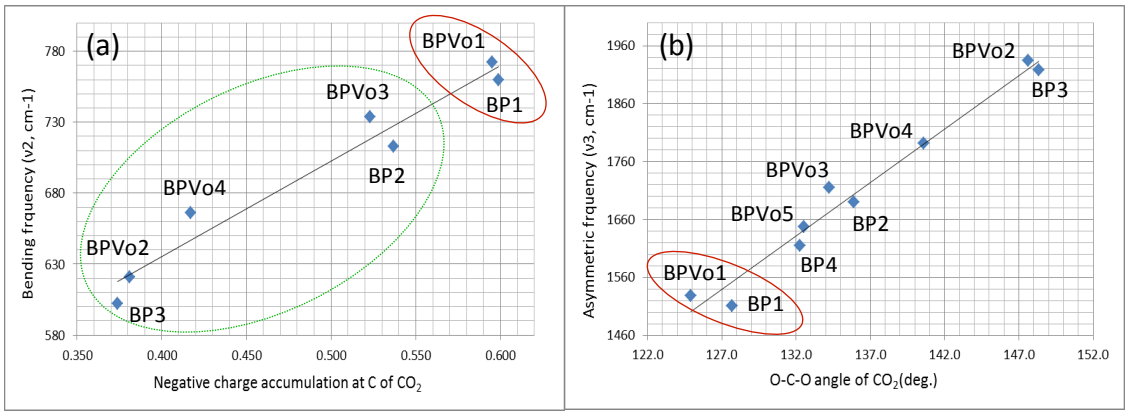

Figure 4. Correlations between (a) the bending frequency (ν2) and the negative charge accumulation at C of CO_2, and of (b) the asymmetric stretching frequency (ν3) and the O-C-O

angle of CO_2. (Red circle: CO_2 adsorption sites at the interface edge; Green dotted circle: CO_2 adsorption sites directly on the Pt octamer.)

In summary, for bent-form CO_2 species associated with the Pt octamer, a higher ν2 mode seems to be an indicator of adsorbed CO_2 with more negative charge accumulation. On the other hand, a higher ν3 mode seems to reveal a larger O-C-O angle of CO_2. Moreover, a ν2 mode below ~800 cm^{-1} tends to indicate CO_2 adsorption sites for which there is direct interaction between the adsorbate at the Pt octamer, whereas direct TiO_2 surface sites show higher ν2 values. Values of ν2 in the range ~750-800 cm^{-1} are primarily associated with interface edge adsorption, whereas values below that range indicate adsorption mainly on the Pt octamer itself. Interface edge adsorption sites may also be revealed by smaller ν3 values (~1500-1540 cm^{-1}).

Note that according to Tables 2 & 3, the calculated frequencies of pairs with similar adsorption configurations (e.g., BP1 & BPVo1, BP2 & BPVo3, and BP3 & BPVo2) are similar to each other. This gives confidence in uniquely assigning frequencies to observed adsorption sites. For instance, on the surfaces with a Pt octamer deposited on anatase TiO_2 (101), we can assign ν1 and ν3 in the ranges of 1174-1203 cm^{-1} and 1511-1529 cm^{-1}, respectively, to an adsorbed CO_2^- anion at the interface edge. The ν1 and ν3 ranges of 1114-1130 cm^{-1} and 1690-1715 cm^{-1} can be assigned to a CO_2^- anion on a Pt octamer involving simultaneous interaction with two Pt atoms. The ν1 and ν3 ranges of 1142-1167 cm^{-1} and 1918-1934 cm^{-1} can be ascribed to a CO_2^- anion on a Pt octamer involving interaction with only one Pt atom.

3.3 Pt octamer induced CO_2 dissociation to CO

So far, we have considered the formation of surface-adsorbed complexes that resemble the CO_2^- anion, which is a key precursor for the formation of CO. In this section, we explore a possible

pathway for the subsequent reduction step, namely, cleavage of CO_2^- to form surface-adsorbed CO on a neutral surface of a reduced anatase TiO_2 (101)-supported Pt octamer.

The dissociation of CO_2 to CO has been investigated by a number of investigators.[55-58] While such dissociation was observed on the surfaces of reduced TiO_2-supported Pt, Rh, and Ir upon illumination at 190K, supported Pd and Ru surfaces exhibited no CO formation.[56] An investigation using an electron-induced route (i.e., electrocatalysis) was also reported on reduced TiO_2 (110) with a threshold of 1.4 eV.[58] Based on DFT calculations, promising photocatalysts such as Zn_2GeO_4 (010)[48] and ceria (110)[50] also suggest the possibility of forming CO from CO_2 dissociation on surfaces with oxygen vacancies. One common feature of the proposed dissociation mechanisms is that one O atom of the CO_2 molecule is linked to the oxygen vacancy, resulting in the weakening of the C-O bond.

Figure 5 shows a possible dissociation pathway (CF1-CF7) for adsorbed CO_2 to adsorbed CO. In the final configuration (CF7), CO is found at the interface edge with C interacting with two Pt atoms at an average distance of 1.94 Å and O with 5c-Ti in a distance of 2.28 Å. The dissociated O bridges a 5c-Ti and a Pt atom at distances of 1.78 Å and 2.01 Å, respectively. To understand the energy needed to activate the CO_2 dissociation, a scenario is investigated starting with CO_2 adsorbed on the TiO_2 surface, shown in CF1 (one of the obtained stable CO_2 adsorption configuration as BPVo5 in Figure 2h). The CI-NEB calculation shows that a disturbance of 0.15eV is initially needed to destabilize the adsorbed CO_2 (CF2), following which the system follows a downhill path to a configuration where C of the CO_2 is interacting with one Pt atom of the Pt octamer (CF3). The major energy barrier (CF4) is then reflected in the extraction of one O from CO_2 to a bond distance of 1.83 Å (for reference, the calculated bond distance of C-O is 1.18 Å for free CO_2), followed by a downhill path to continue the C-O separation and transition to a

configuration in which the C atom interacts with two Pt atoms instead of one (CF5-CF7). The energy barrier of CO_2 dissociation to CO is estimated to be 1.01eV.

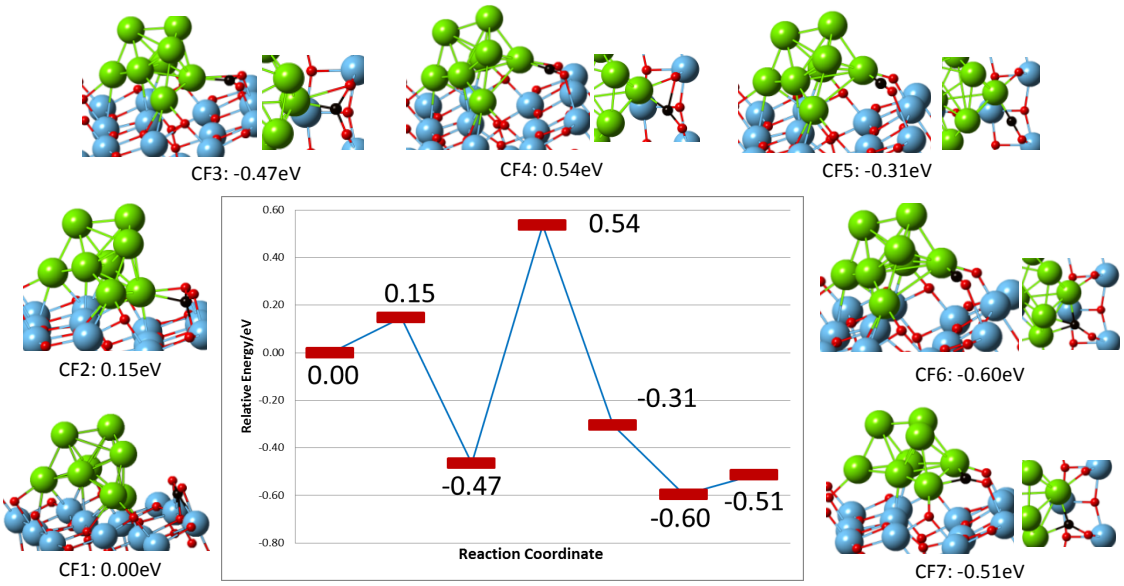

Figure 5. A proposed pathway, CF1-CF7, for CO_2 dissociation to CO on the surface of a reduced anatase TiO_2 (101)-supported Pt octamer.

This mechanism is different from what has been reported for larger nanoparticles, where one O of CO_2 fills the oxygen vacancy as C bonds to the nanoparticle, then upon irradiation transfers the photo-induced charge to the CO_2 molecule to activate C-O bond breaking.[56] In the case of the Pt octamer on reduced anatase (101), our proposed dissociation mechanism is not directly related to filling of the oxygen vacancy. Rather, the key role of the vacancy here is to enable the cluster to more easily modify its geometry to facilitate the dissociation process. This is a direct consequence of the fluxionality of the subnanometer metal cluster, which is not possible for larger particles. This geometric reorganization is best seen in the early steps in the proposed mechanism (CF2-CF4), in which one Pt atom stretches out of the Pt octamer to interact with the CO_2 molecule.

The weakening of the C-O bond is attributed to the filling of antibonding orbitals of the CO_2 molecule.[59] Based on the configurations in Figure 3, it is difficult to uniquely identify the antibonding orbitals, but the highest bonding orbital of CO_2 can be seen in DP4 of Figure 3a and DP2 of Figure 3b, which lie deep below the Fermi level. This suggests that the hybridization of antibonding orbitals of CO_2 could also occur below the Fermi level. For instance, in Figure 3b, states DP3 & DP4 clearly have antibonding character, and could lead to the cleavage of the C-O bond of the CO_2 molecule. This result suggests another possible advantage that Pt octamers or other subnanometer metal clusters may bring to CO_2 photoreduction.

4. Conclusions

The presence of Ag or Pt octamers can substantially modify CO_2 adsorption on perfect & reduced anatase TiO_2 (101) based on DFT calculations. In fact, the presence of the Ag & Pt octamers affects CO_2 adsorption even at TiO_2 surface sites where there is no direct binding between CO_2 and the octamer, suggesting the octamer modifies the properties of the TiO_2 itself as it donates electron density to the surface. For adsorption on the TiO_2 sites not directly abutting the octamers, the nature of the Ag/Pt-induced effect depends on the orientation of the adsorbed CO_2 molecule. It also differs for the perfect (vacancy-free) and reduced (oxygen vacancy) surfaces. We attribute this behavior to a binding mechanism that involves electrostatic competition between two factors: (1) attraction between Ti and the O atom of CO_2 as the latter accepts negative charge from the surface; and (2) repulsion between Ti and the C atom of CO_2.

Deposition of subnanometer Pt clusters appears to provide certain important advantages for CO_2 activation on anatase TiO_2(101) surfaces. First, the Pt atoms provide extra adsorption sites for bent-form CO_2—a key dissociation precursor state leading to the products of CO_2 photoreduction—as compared to the Ag-octamer-decorated or pure anatase TiO_2 (101) surfaces.

The available sites were found at the interface edge of the Pt octamer and the anatase surface, and also directly on the Pt octamer. In most cases, the adsorption strength at these sites is also enhanced, which is generally beneficial for bond activation. In addition, Bader charge analysis suggests that at these Pt surface or Pt-TiO_2 interface sites, the adsorbed CO_2 can be spontaneously converted to a CO_2^- anion-type complex as negative charge accumulates at the C atom of the CO_2 molecule. A detailed examination of the associated electronic structure suggests that unlike binding to TiO_2 sites, where electrostatics play a key role, the interaction between CO_2 and Pt is instead facilitated by the molecular orbitals of CO_2 forming bonding orbitals with d states of Pt in the octamer. This explains the significant charge transfer to the adsorbed CO_2, as well as the Pt octamer's ability to provide additional adsorption sites. This same advantage is lacking for the Ag octamer, likely a consequence of insufficient orbital overlap due to the shape and orientation of the outer s orbitals of Ag.

Calculated vibrational frequencies suggest that the ν2 vibrational mode of bent CO_2 molecules adsorbed on Pt octamers can be used as an indicator of negative charge accumulation on C, and hence the formation of the CO_2^- anion precursor. In addition, a direct relation between the ν3 mode and the O-C-O angle of the CO_2 molecule was found, which provides a possible mechanism for identifying bent CO_2 geometries. Information from the vibrational frequencies can also be used for identification of CO_2 adsorption sites. For instance, a ν2 mode > ~800 cm^{-1} seems to indicate CO_2 adsorption on sites that are not directly associated with the Pt octamer, while lower frequencies correspond to sites that are related to the Pt octamer. Also, ν2 in the ~750-800 cm^{-1} range, combined with a small ν3 (~1500-1540 cm^{-1}), tends to indicate interface edge adsorption.

Finally, we show one possible mechanism by which a Pt octamer on reduced anatase TiO_2 (101) could further dissociate adsorbed CO_2 to CO, aided by the enhanced fluxionality of the Pt octamer due to the oxygen vacancy, and by the filling of antibonding orbitals of CO_2 to weaken the intramolecular C-O bond. The calculated energy barrier for this surface dissociation process is 1.01eV. In summary, our results suggest that subnanometer metal clusters such as Pt could be used to enhance the photocatalytic activity of TiO_2 and other semiconductors.

Acknowledgements

The authors also wish to thank the USF supercomputing center for computing time and support along with XSEDE and NERSC supercomputing resources. A portion of this work was performed under the auspices of the U.S. Department of Energy by Lawrence Livermore National Laboratory under Contract DE-AC52-07NA27344.

Supporting Information

Optimized geometries of CO_2 adsorbed on perfect and reduced anatase (101) surfaces; charge density difference of adsorbed CO_2 on perfect and reduced anatase (101) surfaces in the presence of the Pt octamer. This material is available free of charge via the Internet at http://pubs.acs.org.

References

1. Fujishima, A.; Honda, K., Electrochemical Photolysis of Water at a Semiconductor Electrode. In *Nature*, 1972; pp 37-38.

2. Konstantinou, I. K.; Albanis, T. A., TiO2-assisted photocatalytic degradation of azo dyes in aqueous solution: kinetic and mechanistic investigations - A review. *Applied Catalysis B-Environmental* **2004,** *49*, 1-14.

3. Aurianblajeni, B.; Halmann, M.; Manassen, J., Photo-Reduction of Carbon-Dioxide and Water into Formaldehyde and Methanol on Semiconductor-Materials. *Solar Energy* **1980,** *25*, 165-170.
4. Indrakanti, V. P.; Kubicki, J. D.; Schobert, H. H., Photoinduced activation of CO2 on Ti-based heterogeneous catalysts: Current state, chemical physics-based insights and outlook. *Energy & Environmental Science* **2009,** *2*.
5. Zhang, Q.-H.; Han, W.-D.; Hong, Y.-J.; Yu, J.-G., Photocatalytic reduction of CO2 with H2O on Pt-loaded TiO2 catalyst. *Catalysis Today* **2009,** *148*, 335-340.
6. Sclafani, A.; Herrmann, J.-M., Influence of metallic silver and of platinum-silver bimetallic deposits on the photocatalytic activity of titania (anatase and rutile) in organic and aqueous media. *Journal of Photochemistry and Photobiology A: Chemistry* **1998,** *113*, 181-188.
7. Linic, S.; Christopher, P.; Ingram, D. B., Plasmonic-metal nanostructures for efficient conversion of solar to chemical energy. *Nat Mater* **2011,** *10*, 911-921.
8. Hou, W.; Hung, W. H.; Pavaskar, P.; Goeppert, A.; Aykol, M.; Cronin, S. B., Photocatalytic Conversion of CO2 to Hydrocarbon Fuels via Plasmon-Enhanced Absorption and Metallic Interband Transitions. *ACS Catalysis* **2011,** *1*, 929-936.
9. Varghese, O. K.; Paulose, M.; LaTempa, T. J.; Grimes, C. A., High-Rate Solar Photocatalytic Conversion of CO2 and Water Vapor to Hydrocarbon Fuels. *Nano Letters* **2009,** *9*, 731-737.
10. Wang, J.; Tafen, D. N.; Lewis, J. P.; Hong, Z.; Manivannan, A.; Zhi, M.; Li, M.; Wu, N., Origin of Photocatalytic Activity of Nitrogen-Doped TiO2 Nanobelts. *Journal of the American Chemical Society* **2009,** *131*, 12290-12297.
11. Kočí, K.; Matějů, K.; Obalová, L.; Krejčíková, S.; Lacný, Z.; Plachá, D.; Čapek, L.; Hospodková, A.; Šolcová, O., Effect of silver doping on the TiO2 for photocatalytic reduction of CO2. *Applied Catalysis B: Environmental* **2010,** *96*, 239-244.
12. Christopher, P.; Ingram, D. B.; Linic, S., Enhancing Photochemical Activity of Semiconductor Nanoparticles with Optically Active Ag Nanostructures: Photochemistry Mediated by Ag Surface Plasmons. *The Journal of Physical Chemistry C* **2010,** *114*, 9173-9177.
13. Lei, Y.; Mehmood, F.; Lee, S.; Greeley, J.; Lee, B.; Seifert, S.; Winans, R. E.; Elam, J. W.; Meyer, R. J.; Redfern, P. C.; Teschner, D.; Schlögl, R.; Pellin, M. J.; Curtiss, L. A.; Vajda, S., Increased Silver Activity for Direct Propylene Epoxidation via Subnanometer Size Effects. *Science* **2010,** *328*, 224-228.
14. Yoon, B.; Häkkinen, H.; Landman, U.; Wörz, A. S.; Antonietti, J.-M.; Abbet, S.; Judai, K.; Heiz, U., Charging Effects on Bonding and Catalyzed Oxidation of CO on Au8 Clusters on MgO. *Science* **2005,** *307*, 403-407.
15. Qiao, B. T.; Wang, A. Q.; Yang, X. F.; Allard, L. F.; Jiang, Z.; Cui, Y. T.; Liu, J. Y.; Li, J.; Zhang, T., Single-atom catalysis of CO oxidation using Pt-1/FeOx. *Nat Chem* **2011,** *3*, 634-641.
16. Hakkinen, H.; Abbet, W.; Sanchez, A.; Heiz, U.; Landman, U., Structural, electronic, and impurity-doping effects in nanoscale chemistry: Supported gold nanoclusters. *Angewandte Chemie-International Edition* **2003,** *42*, 1297-1300.
17. Vajda, S.; Pellin, M. J.; Greeley, J. P.; Marshall, C. L.; Curtiss, L. A.; Ballentine, G. A.; Elam, J. W.; Catillon-Mucherie, S.; Redfern, P. C.; Mehmood, F.; Zapol, P., Subnanometre platinum clusters as highly active and selective catalysts for the oxidative dehydrogenation of propane. *Nat Mater* **2009,** *8*, 213-216.
18. TAUSTER, S. J., Strong Metal-Support Interactions. *Accounts Chem Res* **1987,** *20*.
19. Han, Y.; Liu, C.-j.; Ge, Q., Interaction of Pt Clusters with the Anatase TiO2(101) Surface: A First Principles Study. *The Journal of Physical Chemistry B* **2006,** *110*, 7463-7472.
20. Mazheika, A. S.; Matulis, V. E.; Ivashkevich, O. A., Quantum chemical study of adsorption of Ag2, Ag4 and Ag8 on stoichiometric TiO2 (100) surface. *Journal of Molecular Structure: THEOCHEM* **2010,** *942*, 47-54.

21. Yang, C.-T.; Balakrishnan, N.; Bhethanabotla, V. R.; Joseph, B., Interplay between Subnanometer Ag and Pt Clusters and Anatase TiO2 (101) Surface: Implications for Catalysis and Photocatalysis. *The Journal of Physical Chemistry C* **2014,** *118*, 4702-4714.
22. Çakır, D.; Gülseren, O., Adsorption of Pt and Bimetallic PtAu Clusters on the Partially Reduced Rutile (110) TiO2Surface: A First-Principles Study. *The Journal of Physical Chemistry C* **2012,** *116*, 5735-5746.
23. Henderson, M. A., A surface science perspective on TiO(2) photocatalysis. *Surface Science Reports* **2011,** *66*, 185-297.
24. Usubharatana, P.; McMartin, D.; Veawab, A.; Tontiwachwuthikul, P., Photocatalytic Process for CO2 Emission Reduction from Industrial Flue Gas Streams. *Industrial & Engineering Chemistry Research* **2006,** *45*, 2558-2568.
25. He, H.; Zapol, P.; Curtiss, L. A., A Theoretical Study of CO2 Anions on Anatase (101) Surface. *The Journal of Physical Chemistry C* **2010,** *114*, 21474-21481.
26. Indrakanti, V. P.; Schobert, H. H.; Kubicki, J. D., Quantum Mechanical Modeling of CO2 Interactions with Irradiated Stoichiometric and Oxygen-Deficient Anatase TiO2 Surfaces: Implications for the Photocatalytic Reduction of CO2. *Energy & Fuels* **2009,** *23*, 5247-5256.
27. Rodriguez, M. M.; Peng, X. H.; Liu, L. J.; Li, Y.; Andino, J. M., A Density Functional Theory and Experimental Study of CO2 Interaction with Brookite TiO2. *J Phys Chem C* **2012,** *116*, 19755-19764.
28. Freund, H. J.; Roberts, M. W., Surface chemistry of carbon dioxide. *Surface Science Reports* **1996,** *25*, 225-273.
29. Indrakanti, V. P.; Kubicki, J. D.; Schobert, H. H., Quantum Chemical Modeling of Ground States of CO 2 Chemisorbed on Anatase (001), (101), and (010) TiO 2 Surfaces. *Energy & Fuels* **2008,** *22*, 2611-2618.
30. Markovits, A.; Fahmi, A.; Minot, C., A theoretical study of CO2 adsorption on TiO2. *Journal of Molecular Structure: THEOCHEM* **1996,** *371*, 219-235.
31. Dan C. Sorescu, W. A. A.-S., and Kenneth D. Jordan, CO2 adsorption on TiO2(101) anatase: A dispersion-corrected density functional theory study. *Journal of Chemical Physics* **2011,** *135*, 124701.
32. Selloni, A., Crystal growth: Anatase shows its reactive side. *Nat Mater* **2008,** *7*, 613-615.
33. Gong, X. Q.; Selloni, A.; Dulub, O.; Jacobson, P.; Diebold, U., Small au and pt clusters at the anatase TiO2(101) surface: Behavior at terraces, steps, and surface oxygen vacancies. *J Am Chem Soc* **2008,** *130*, 370-381.
34. Zhou, Y.; Muhich, C. L.; Neltner, B. T.; Weimer, A. W.; Musgrave, C. B., Growth of Pt Particles on the Anatase TiO2 (101) Surface. *J Phys Chem C* **2012,** *116*, 12114-12123.
35. Perdew, J. P.; Burke, K.; Ernzerhof, M., Generalized gradient approximation made simple. *Phys. Rev. Lett.* **1996,** *77*, 3865-3868.
36. Kresse, G.; Furthmuller, J., Efficiency of ab-initio total energy calculations for metals and semiconductors using a plane-wave basis set. *Comp. Mater. Sci.* **1996,** *6*, 15-50.
37. Kresse, G.; Furthmuller, J., Efficient iterative schemes for ab initio total-energy calculations using a plane-wave basis set. *Phys. Rev. B: Condens. Matter Mater. Phys.* **1996,** *54*, 11169-11186.
38. Kresse, G.; Hafner, J., ABINITIO MOLECULAR-DYNAMICS FOR LIQUID-METALS. *Phys. Rev. B: Condens. Matter Mater. Phys.* **1993,** *47*, 558-561.
39. Blochl, P. E., PROJECTOR AUGMENTED-WAVE METHOD. *Phys. Rev. B: Condens. Matter Mater. Phys.* **1994,** *50*, 17953-17979.
40. Monkhorst, H. J.; Pack, J. D., SPECIAL POINTS FOR BRILLOUIN-ZONE INTEGRATIONS. *Phys. Rev. B: Condens. Matter Mater. Phys.* **1976,** *13*, 5188-5192.
41. Sanville, E.; Kenny, S. D.; Smith, R.; Henkelman, G., Improved grid-based algorithm for Bader charge allocation. *J Comput Chem* **2007,** *28*, 899-908.

42. Sheppard, D.; Terrell, R.; Henkelman, G., Optimization methods for finding minimum energy paths. *Journal of Chemical Physics* **2008,** *128*.
43. Henkelman, G.; Jonsson, H., Improved tangent estimate in the nudged elastic band method for finding minimum energy paths and saddle points. *J Chem Phys* **2000,** *113*, 9978-9985.
44. Henkelman, G.; Uberuaga, B. P.; Jonsson, H., A climbing image nudged elastic band method for finding saddle points and minimum energy paths. *J Chem Phys* **2000,** *113*, 9901-9904.
45. Ammal, S. C.; Heyden, A., Modeling the noble metal/TiO2 (110) interface with hybrid DFT functionals: A periodic electrostatic embedded cluster model study. *J Chem Phys* **2010,** *133*.
46. Mazheika, A. S.; Bredow, T.; Matulis, V. E.; Ivashkevich, O. A., Theoretical Study of Adsorption of Ag Clusters on the Anatase TiO2(100) Surface. *J Phys Chem C* **2011,** *115*, 17368-17377.
47. Chretien, S.; Metiu, H., Density functional study of the interaction between small Au clusters, Au[sub n] (n = 1 - 7) and the rutile TiO[sub 2] surface. I. Adsorption on the stoichiometric surface[J. Chem. Phys. [bold 127], 084704 (2007)]. *The Journal of Chemical Physics* **2007,** *127*, 149902-1.
48. Liu, L.; Fan, W. L.; Zhao, X.; Sun, H. G.; Li, P.; Sun, L. M., Surface Dependence of CO2 Adsorption on Zn2GeO4. *Langmuir* **2012,** *28*, 10415-10424.
49. Rodriguez, M. M.; Peng, X. H.; Liu, L. J.; Li, Y.; Andino, J. M., A Density Functional Theory and Experimental Study of CO2 Interaction with Brookite TiO2. In *J Phys Chem C*, 2012; pp 19755-19764.
50. Cheng, Z.; Sherman, B. J.; Lo, C. S., Carbon dioxide activation and dissociation on ceria (110): A density functional theory study. *J Chem Phys* **2013,** *138*.
51. Hartman, K. O.; Hisatsun.Ic, Infrared Spectrum of Carbon Dioxide Anion Radical. *J Chem Phys* **1966,** *44*, 1913-&.
52. Ramis, G.; Busca, G.; Lorenzelli, V., Low-Temperature Co-2 Adsorption on Metal-Oxides - Spectroscopic Characterization of Some Weakly Adsorbed Species. *Mater Chem Phys* **1991,** *29*, 425-435.
53. Rasko, J.; Solymosi, F., Infrared Spectroscopic Study of the Photoinduced Activation of CO2 on TiO2 and Rh/TiO2 Catalysts. *The Journal of Physical Chemistry* **1994,** *98*, 7147-7152.
54. Su, W. G.; Zhang, J.; Feng, Z. C.; Chen, T.; Ying, P. L.; Li, C., Surface phases of TiO2 nanoparticles studied by UV Raman spectroscopy and FT-IR spectroscopy. *J Phys Chem C* **2008,** *112*, 7710-7716.
55. Liu, L. J.; Zhao, H. L.; Andino, J. M.; Li, Y., Photocatalytic CO2 Reduction with H2O on TiO2 Nanocrystals: Comparison of Anatase, Rutile, and Brookite Polymorphs and Exploration of Surface Chemistry. *Acs Catalysis* **2012,** *2*, 1817-1828.
56. Rasko, J., FTIR study of the photoinduced dissociation of CO2 on titania-supported noble metals. *Catalysis Letters* **1998,** *56*, 11-15.
57. Rasko, J.; Solymosi, F., Infrared Spectroscopic Study of the Photoinduced Activation of Co2 on Tio2 and Rh/Tio2 Catalysts. *Journal of Physical Chemistry* **1994,** *98*, 7147-7152.
58. Lee, J.; Sorescu, D. C.; Deng, X. Y., Electron-Induced Dissociation of CO2 on TiO2(110). *Journal of the American Chemical Society* **2011,** *133*, 10066-10069.
59. Nilsson, A.; Pettersson, L. G. M.; Hammer, B.; Bligaard, T.; Christensen, C. H.; Norskov, J. K., The electronic structure effect in heterogeneous catalysis. *Catal Lett* **2005,** *100*, 111-114.